Right atrial volumes and strains in healthy adults: is the Frank-Starling mechanism working?—detailed analysis from the three-dimensional speckle-tracking echocardiographic MAGYAR-Healthy Study

Attila Nemes, Árpád Kormányos

Department of Medicine, Albert Szent-Györgyi Medical School, University of Szeged, Szeged, Hungary

Contributions: (I) Conception and design: A Nemes; (II) Administrative support: Á Kormányos; (III) Provision of study materials or patients: Both authors; (IV) Collection and assembly of data: Both authors; (V) Data analysis and interpretation: Both authors; (VI) Manuscript writing: Both authors; (VII) Final approval of manuscript: Both authors.

Correspondence to: Attila Nemes, MD, PhD, DSc, FESC. Department of Medicine, Albert Szent-Györgyi Medical School, University of Szeged, Semmelweis Street 8, H-6725 Szeged, Hungary. Email: nemes.attila@med.u-szeged.hu.

Background: With larger blood volume flowing into a cardiac chamber, by stretching muscle fibers, increased contraction force could be detected. This phenomenon is called Frank-Starling mechanism, allowing the output of a cardiac chamber to be synchronized without external regulation. The purpose of the present study was to investigate the Frank-Starling mechanism in the right atrium (RA) represented by its volumes, volume-based functional properties and strains respecting the cardiac cycle in healthy adults by three-dimensional (3D) speckle-tracking echocardiography (3DSTE).

Methods: The present single center retrospective cohort study comprised 179 healthy adult volunteers (mean age: 33.2 ± 12.0 years, 92 males), in whom complete two-dimensional Doppler echocardiography with 3DSTE was performed. Subjects were divided into 3 groups according to the mean value of maximum RA volume (V_{max}) ± standard deviation: $V_{max} <30$ mL, 30 mL $\leq V_{max} <60$ mL and $V_{max} \geq 60$ mL.

Results: All RA volumes respecting the cardiac cycle of all subjects and calculated separately for females and males and their indexed equivalents increased with V_{max}. RA stroke volumes increased with V_{max} regardless of the phase it was measured in. While total atrial emptying fraction representing the reservoir phase remained unchanged with the increase of V_{max}, a significant increase in passive atrial emptying fraction representing the conduit phase could be detected, in case of $V_{max} >60$ mL ($28.9\% \pm 15.1\%$ *vs.* $32.5\% \pm 12.6\%$, P<0.05). Active atrial emptying fraction representing the booster pump function did not change with the increase of V_{max}. Most global and mean segmental peak RA strains did not show significant changes with increasing RA volumes except for the RA area strain, it was the largest when V_{max} was larger than 60 mL ($64.7\% \pm 44.9\%$ *vs.* $83.3\% \pm 49.4\%$, P<0.05). RA circumferential, longitudinal and area strains at atrial contraction decreased with increasing V_{max}, RA radial and 3D strains did not change significantly with increasing V_{max}.

Conclusions: Increasing RA volumes do not cause significant increase in RA contractility represented by strains, but reduction in strains in longitudinal and circumferential directions could be detected in end-diastolic booster pump function. In contrast to the left atrium, obvious signs of Frank-Starling mechanism could not be detected in case of the RA.

Keywords: Healthy; right atrial; strain; three-dimensional (3D); echocardiography

Introduction

With larger blood volume flowing into a cardiac chamber, by stretching muscle fibers, increased contraction force could be detected (1). This phenomenon is called the Frank-Starling mechanism, allowing the output of a cardiac chamber to be synchronized without external regulation (1). This sort of relationship could be demonstrated not only for the left ventricle (LV) (2), but for the left atrium (LA), as well (3,4). In recent studies, increased LA contractility facilitated by increased LA preload could be seen, however, only up to a point, beyond which LA contractility did not increase further (3,4). Similar detailed analysis for the right atrium (RA), however, was not performed. Novel cardiovascular imaging methods including three-dimensional speckle-tracking echocardiography (3DSTE) allows detailed analysis of such relationships in a non-invasive way even in healthy subjects (5-7). The present study aimed to investigate the Frank-Starling mechanism in the RA represented by its volumes, volume-based functional properties and strains respecting the cardiac cycle in healthy adults by 3DSTE.

Methods

Study population

The present single center retrospective cohort study consisted of 179 healthy adults (mean age: 33.2±12.0 years, 92 males), in case of whom laboratory, electrocardiographic and echocardiographic findings were normal. They had no symptoms, drug use, known disorders or any pathological signs, which could theoretically affect the results. None of the healthy subjects were athletes or had performed significant or prolonged exercise 1 week before 3DSTE examinations. All subjects had undergone complete two-dimensional (2D) Doppler echocardiographic examination extended with 3DSTE-derived echocardiographic data acquisition. 3DSTE-derived data analysis was performed at a later date offline (8-10). 3DSTE data acquisitions and analyses were performed in the 3D echocardiographic laboratory at the University of Szeged with 12-year experience with 3D echocardiography. All data were analysed by two experienced physicians (AN, ÁK). The present study is a part of the Motion Analysis of the heart and Great vessels bY three-dimensionAl speckle-tRacking echocardiography in Healthy subjects (MAGYAR-Healthy) Study, which was organized for physiologic studies among others following acquisition of 3D echocardiographic datasets of hundreds of healthy adults ('Magyar' means 'Hungarian' in Hungarian language) (3,5,8,9). The study was conducted in accordance with the Declaration of Helsinki (as revised in 2013). The study was approved by the Institutional and Regional Human Biomedical Research Committee of University of Szeged (Hungary) (No. 71/2011 and updated versions) and informed consent was taken from all the subjects.

2D Doppler echocardiography

In case of all subjects, before preparing the 3DSTE, complete 2D Doppler echocardiography was performed to exclude significant abnormalities and to assess routine parameters. Toshiba Artida™ echocardiographic machine (Toshiba Medical Systems, Tokyo, Japan) was used in all cases attached with a PST-30BT (1–5 MHz) phased-array transducer. LV and LA quantifications were performed according to recent guidelines. Right ventricular fractional area change (RV-FAC) and tricuspid annular plane systolic excursion (TAPSE) were also measured (11). Doppler echocardiography was used for valvular assessments and to determine early (E) and late (A) mitral inflow velocities. Following determination of early diastolic myocardial flow velocity (E') by tissue Doppler echocardiography, E/E' was also assessed as a feature of diastolic function.

3D speckle-tracking echocardiography

For 3DSTE studies, the same Toshiba Artida™ echocardiographic machine (Toshiba Medical Systems, Tokyo, Japan) was used with a PST-25SX phased-array matrix transducer with 3D capability (8-10). Firstly, 3D echocardiographic dataset was digitally acquired with 26.8±1.1 vps from the apical window, offline analysis was performed at a later date. Six RA-focused sub-volumes were acquired within 6 cardiac cycles, during a single breath-hold, from which a pyramid-shape 3D full volume was
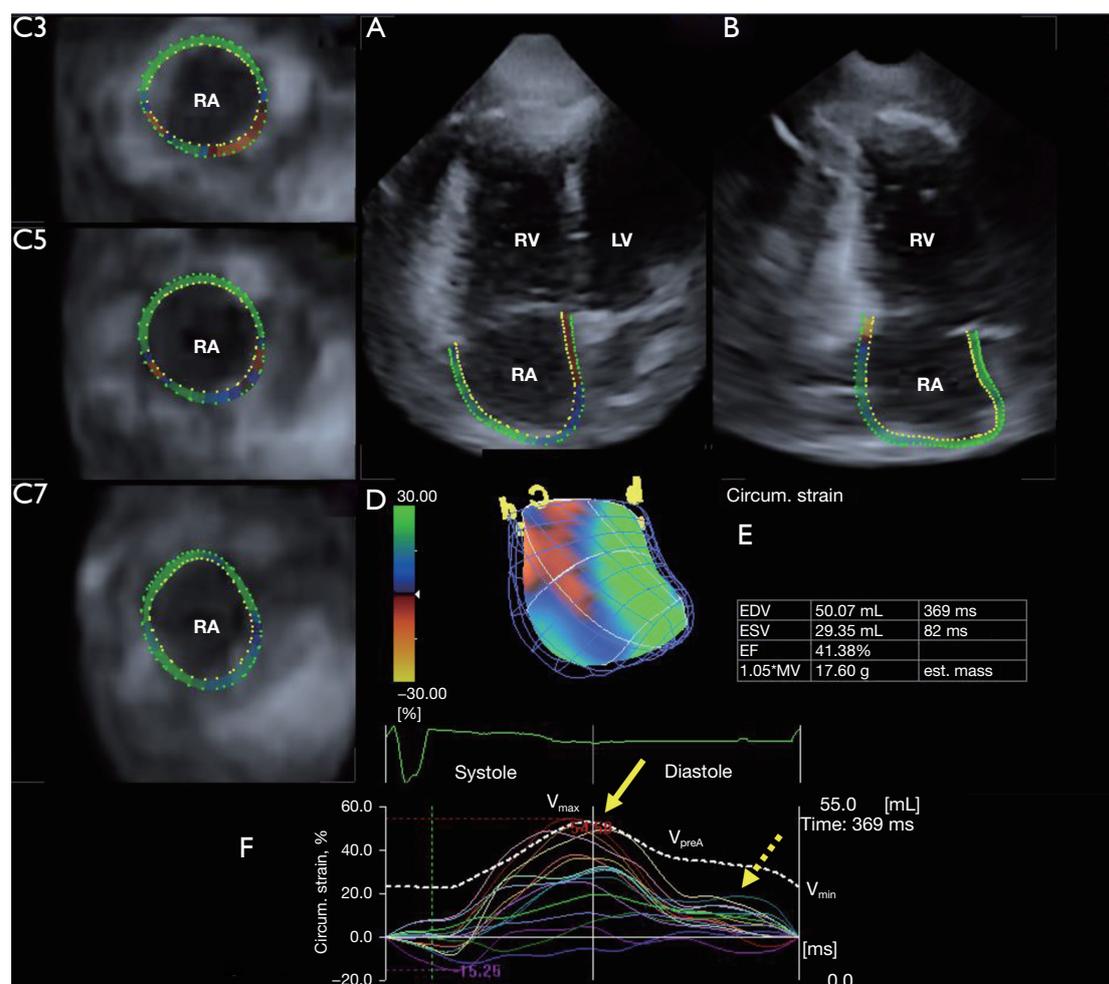
Figure 1 3D speckle-tracking echocardiographic RA analysis in a healthy subject is demonstrated: apical longitudinal four-chamber (A) and two-chamber views (B) and short-axis views at basal (C3), midatrial (C5) and superior (C7) RA levels. 3D cast of the RA (D), calculated RA volumetric data (E) and time – global RA volume change (dashed line) and time – segmental RA circumferential strain curves (coloured lines) respecting the cardiac cycle are presented (F). Peak RA strains are represented by yellow arrows, while RA strains at atrial contraction are represented by dotted yellow arrow. 3D, three-dimensional; LV, left ventricle; RA; right atrium; RV, right ventricle; EDV, end-diastolic volume; ESV, end-systolic volume; EF, ejection fraction; est., estimated; MV, myocardial volume; V_{max}, maximum right atrial volume; V_{preA}, volume at the onset of atrial systole; V_{min}, minimum right atrial volume.

automatically created. RA was examined with the help of auxiliary apical 4-chamber (AP4CH) and 2-chamber (AP2CH) longitudinal views and short-axis views focused on the basal, mid-atrial, and superior RA regions (*Figure 1*) with the help of 3D Wall Motion Tracking software version 2.7 (Toshiba Medical Systems, Tokyo, Japan). In longitudinal views, reference points at the lateral edge of RA-tricuspid annulus (TA) moving towards the septal edge of the RA-TA were traced. RA appendage, superior and inferior venae cava and coronary sinus were excluded from

the measurements. 3D wall motion tracking helped creation of the virtual 3D RA model (8-10).

The following RA volumes were determined (8,10):

❖ End-systolic maximum RA volume (V_{max}, at the time of tricuspid valve opening);

❖ RA volume at the onset of atrial systole (V_{preA}, at the p wave on electrocardiography);

❖ End-diastolic minimum RA volume (V_{min}, at tricuspid valve closure).

The following RA volume-based functional properties

were determined (8,10):

- ❖ Systolic reservoir function;
  - ◆ RA total stroke (emptying) volume (TASV = $V_{max} - V_{min}$);
  - ◆ RA total atrial emptying fraction (TAEF = TASV/V_{max}).
- ❖ Early diastolic conduit function;
  - ◆ RA passive stroke (emptying) volume (PASV = $V_{max} - V_{preA}$);
  - ◆ RA passive atrial emptying fraction (PAEF = PASV/V_{max}).
- ❖ Late diastolic booster pump function or active contraction phase.
  - ◆ RA active atrial stroke (emptying) volume (AASV) = $V_{preA} - V_{min}$);
  - ◆ RA active atrial emptying fraction (AAEF) = AASV/V_{preA}).

The following RA strains were determined at RA reservoir function in end-systole (peak strain) and at atrial contraction in end-diastole (at RA systole) (9,10):

- ❖ Radial strain (RS) representing thickening/thinning of a certain RA segment;
- ❖ Longitudinal strain (LS) representing lengthening/shortening of a certain RA segment;
- ❖ Circumferential strain (CS) representing widening/narrowing a certain RA segment;
- ❖ Area strain (AS) is a combination of LS and CS;
- ❖ 3D strain (3DS) is a combination of RS, LS and CS.

Global (assessing the whole RA) and mean segmental values (average of 16 segmental strains) were also calculated. Using twin-peak RA strain curves, the first peak represented the RA systolic reservoir phase, while the second peak represented RA atrial contraction.

According to recent data about normal reference values of maximum end-systolic RA volume, healthy subjects were classified into 3 groups: estimated mean ± standard deviation (SD) served as the lower (30 mL) and upper (60 mL) values (8).

Statistical analysis

Continuous data were presented as mean ± SD, while categorical data were shown as frequencies and percentage, where appropriate. P value less than 0.05 was considered significant. Normality of distribution was evaluated by Shapiro-Wilks test, followed by Levene's test to assess variance of homogeneity. Analysis of variance (ANOVA) was used for normally distributed datasets and Mann-Whitney Wilcoxon test was used in other cases. For categorical variables Fisher's exact test was used. Linear regression plots showing associations between Vmax and peak RA strains have been created. Statistical analysis was done by Medcalc software (Mariakerke, Belgium).

Results

2D Doppler echocardiography

LV end-diastolic and end-systolic diameters (48.0±3.5 and 32.2±3.4 mm, respectively), volumes (105.0±27.2 and 37.9±10.6 mL, respectively), interventricular septal thickness and LV posterior wall (9.0±1.1 and 9.3±1.3 mm, respectively), LV ejection fraction (64.6%±3.5%) and LA diameter in the parasternal long-axis view (37.6±3.6 mm) were measured. All these parameters were in the normal range. Mean transmitral E/A and E/E' ratios were 1.43±0.33 and 8.6±3.2, respectively. Diastolic dysfunction could be detected in 55 out of 179 subjects (31%). RV-FAC and TAPSE were 24.6±3.1 mm and 44.5%±5.4%, respectively. More/equal than grade 1 valvular regurgitation and significant valvular stenosis were excluded in all subjects.

3DSTE-derived LV data

3DSTE-derived LV end-systolic and end-diastolic volumes, indexed volumes, LV mass, indexed LV mass, and LV ejection fraction were 87.1±24.2 mL, 37.0±11.2 mL, 46.0±12.2 mL/m^2, 19.1±6.0 mL/m^2, 155±35 g, 82±16 g/m^2 and 57.6%±4.7%, respectively.

3DSTE-derived RA volumetric data

Subjects were integrated into 3 groups according to the mean value of V_{max} ± SD: V_{max} <30 mL, 30 mL ≤ V_{max} ≤60 mL and >60 mL. No differences between demographic parameters could be detected between the groups examined. All RA volumes respecting the cardiac cycle of all cases and calculated separately for females and males and their indexed equivalents increased with V_{max} (*Table 1*). RA stroke volumes increased with V_{max} regardless of the phase it was measured in. While TAEF representing the reservoir phase remained unchanged with the increase of V_{max}, a significant increase in PAEF representing the conduit phase could be detected, in case of V_{max} >60 mL. AAEF representing the booster pump function did not change with the increase of V_{max} (*Table 2*).

Table 1 Right atrial volumes in healthy cases with different maximum right atrial volumes as assessed by three-dimensional speckle-tracking echocardiography

Variables	V_{max} <30 mL (n=19)	30 mL ≤ V_{max} ≤60 mL (n=129)	V_{max} >60 mL (n=31)
V_{max} (mL)	26.6±3.2	44.4±5.4*	70.9±8.4*†
V_{max}-indexed (mL/m^2)	14.1±2.9	24.4±5.4*	37.7±4.6*†
V_{max} (males) (mL)	26.0±3.5	44.6±8.4*	72.1±8.2*†
V_{max}-indexed (males) (mL/m^2)	12.7±2.6	22.1±4.6*	36.3±3.7*†
V_{max} (females) (mL)	28.1±1.8	44.3±8.3*	69.5±8.7*†
V_{max}-indexed (females) (mL/m^2)	16.5±1.6	26.4±5.2*	39.2±5.1*†
V_{preA} (mL)	19.1±4.9	32.6±7.8*	47.7±9.6*†
V_{preA}-indexed (mL/m^2)	10.0±3.6	18.0±4.9*	25.2±5.2*†
V_{preA} (males) (mL)	18.0±4.9	32.0±7.8*	48.4±10.7*†
V_{preA}-indexed (males) (mL/m^2)	8.5±3.0	16.1±4.0*	24.2±5.6*†
V_{preA} (females) (mL)	21.3±4.6	33.1±7.8*	46.8±8.4*†
V_{preA}-indexed (females) (mL/m^2)	12.5±3.2	19.7±4.9*	26.3±4.8*†
V_{min} (mL)	14.4±3.9	25.3±7.8*	37.4±8.2*†
V_{min}-indexed (mL/m^2)	7.6±2.8	14.0±4.7*	19.9±4.5*†
V_{min} (males) (mL)	13.7±3.4	24.7±7.8*	36.9±8.9*†
V_{min}-indexed (males) (mL/m^2)	6.5±2.0	12.4±7.8*	18.7±4.6*†
V_{min} (females) (mL)	16.1±4.6	25.8±7.7*	38.0±7.5*†
V_{min}-indexed (females) (mL/m^2)	9.5±3.1	15.4±4.9*	21.3±4.1*†

Data are presented as mean ± standard deviation. *, P<0.05 vs. V_{max} <30 mL; †, P<0.05 vs. 30 mL ≤ V_{max} ≤60 mL. V_{max}, maximum right atrial volume; V_{preA}, right atrial volume at the onset of atrial systole; V_{min}, minimum right atrial volume.

3DSTE-derived RA strains

Most global and mean segmental peak RA strains did not show significant changes with increasing RA volumes except for RA-AS, it was the largest when V_{max} was larger than 60 mL. While RA-CS, RA-LS and RA-AS at atrial contraction decreased with increasing V_{max}, RA-RS and RA-3DS did not change significantly with increasing V_{max} (*Figures 2,3*). Linear regression plots showing associations between V_{max} and peak RA-RS, RA-LS, RA-CS, RA-AS, and RA-3DS are demonstrated in *Figures 4,5*.

Inter- and intraobserver variability

The mean difference in values obtained by two observers for the measurements of V_{max}, V_{preA}, V_{min} and peak RA-RS, RA-LS, RA-CS, RA-AS and RA-3DS were 1.0±5.2 mL, −1.5±8.3 mL, 0.9±4.6 mL, −3.5%±12.1%, 5.4%±15.5%, 0.8%±8.6%, 10.4%±36.3% and −1.6%±10.2% respectively, with a correlation coefficient between these independent measurements of 0.96 (P<0.0001), 0.89 (P<0.0001), 0.94 (P<0.0001), 0.68 (P=0.004), 0.77 (P<0.0001), 0.66 (P=0.003), 0.64 (P=0.004) and 0.66 (P=0.007), respectively (interobserver variability). The mean difference in values obtained by 2 measurements of observer 1 for the same parameters proved to be 1.1±6.8 mL, −1.6±9.3 mL, 0.6±5.5 mL, −1.5%±10.3%, 5.6%±18.2%, 1.5%±14.3%, 5.1%±38.3% and 1.1%±10.2% respectively, with a correlation coefficient between these independent measurements of 0.97 (P<0.0001), 0.87 (P<0.0001), 0.96 (P<0.0001), 0.74 (P=0.0007), 0.75 (P=0.0001), 0.60 (P=0.04), 0.73 (P=0.001) and 0.72 (P=0.002), respectively (intraobserver variability).

Table 2 Right atrial volume-based functional properties in healthy cases with different maximum right atrial dimensions as assessed by three-dimensional speckle-tracking echocardiography

Variables	V_{max} <30 mL (n=19)	30 mL ≤ V_{max} ≤60 mL (n=129)	V_{max} >60 mL (n=31)
TASV (mL)	12.2±3.5	19.2±7.5*	33.6±9.6*†
TASV-indexed (mL/m²)	6.5±2.1	10.4±4.3*	17.8±5.3*†
TASV (males) (mL)	12.3±3.2	19.8±7.2*	35.3±7.6*†
TASV-indexed (males) (mL/m²)	6.3±1.9	9.7±3.8*	17.6±3.8*†
TASV (females) (mL)	12.0±4.3	18.5±7.8*	31.5±11.4*†
TASV-indexed (females) (mL/m²)	7.0±2.4	11.0±4.6*	18.0±6.6*†
PASV (mL)	7.6±3.9	11.9±6.0*	23.2±9.6*†
PASV-indexed (mL/m²)	4.1±2.0	6.4±3.3*	12.5±5.3*†
PASV (males) (mL)	8.0±3.8	12.6±5.8*	23.7±9.2*†
PASV-indexed (males) (mL/m²)	4.2±1.8	6.1±3.0	12.1±4.9*†
PASV (females) (mL)	6.8±4.3	11.2±6.2	22.6±10.4*†
PASV-indexed (females) (mL/m²)	4.0±2.5	6.7±3.6	12.9±6.0*†
AASV (mL)	4.7±2.1	7.3±4.4*	10.3±5.2*†
AASV-indexed (mL/m²)	2.4±1.3	4.0±2.6*	5.3±2.7*†
AASV (males) (mL)	4.4±2.5	7.3±4.3*	11.6±5.7*†
AASV-indexed (males) (mL/m²)	2.1±1.5	3.7±2.3*	5.5±3.0*†
AASV (females) (mL)	5.2±0.9	7.3±4.4	8.9±4.1*
AASV-indexed (females) (mL/m²)	3.0±0.6	4.3±2.8	5.0±2.4
TAEF (%)	46.1±12.2	43.0±13.9	47.1±11.6
TAEF (males) (%)	47.6±11.0	44.6±13.6	49.0±10.5
TAEF (females) (%)	42.9±15.0	41.5±14.2	44.7±12.8
PAEF (%)	28.9±15.1	26.5±12.2	32.5±12.6†
PAEF (males) (%)	31.0±15.2	28.0±11.8	32.9±12.4
PAEF (females) (%)	24.3±15.3	25.1±12.5	32.0±13.3
AAEF (%)	23.9±7.9	22.7±12.5	21.6±9.3
AAEF (males) (%)	23.3±8.9	23.3±12.6	23.8±10.5
AAEF (females) (%)	25.3±5.6	22.2±12.4	18.8±7.1

Data are presented as mean ± standard deviation. *, P<0.05 *vs.* V_{max} <30 mL; †, P<0.05 *vs.* 30 mL ≤ V_{max} ≤60 mL. V_{max}, maximum right atrial volume; AASV, active atrial stroke volume; PASV, passive atrial stroke volume; TASV, total atrial stroke volume; AAEF, active atrial emptying fraction; PAEF, passive atrial emptying fraction; TAEF, total atrial emptying fraction.

Discussion

The RA is located on right side of the heart and has a unique structure and morphology with an appendage (12). Its wall is thin, the posterior wall of the RA is smooth, while the anterior part is formed by the pectinate muscles. Superior and inferior caval veins, sinus coronarius and smaller veins enter into the RA, while blood passes to the RV through the tricuspid valve. The RA has a special role in the pacemaker function (sinus node) and conduction as well (12,13). Due to its complex structure and function, there is a limited opportunity for its non-invasive clinical evaluation.
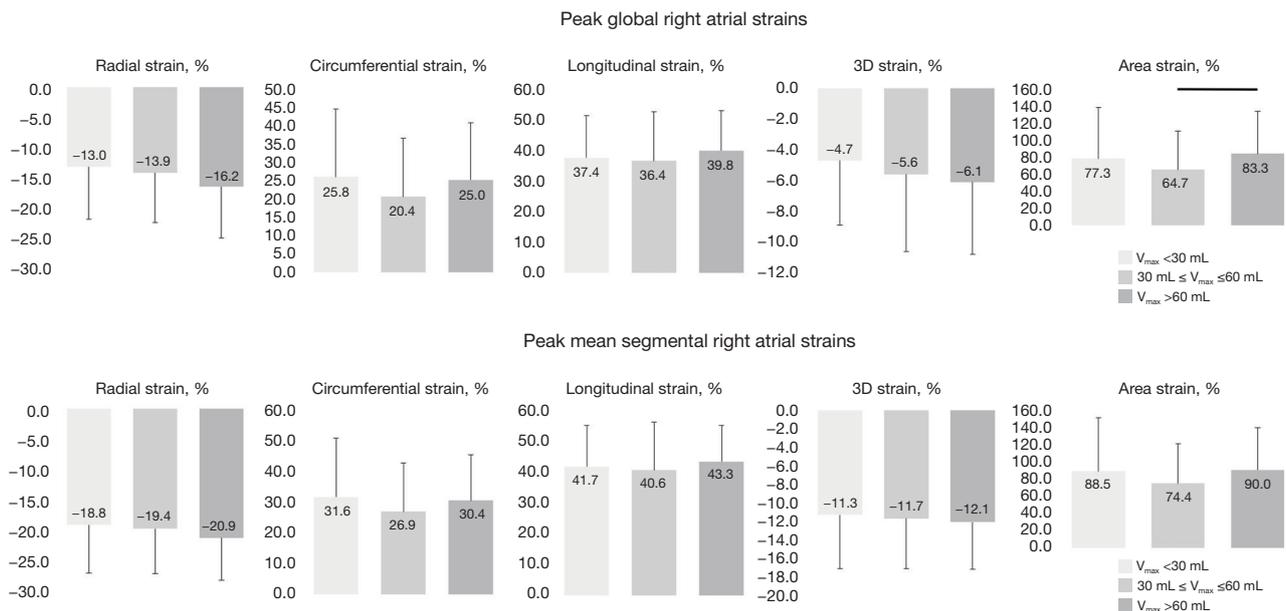
Peak global right atrial strains

Peak mean segmental right atrial strains

Figure 2 Peak global and mean segmental right atrial strains are presented in different maximum right atrial volume groups. 3D, three-dimensional; V_{max}, maximum right atrial volume.
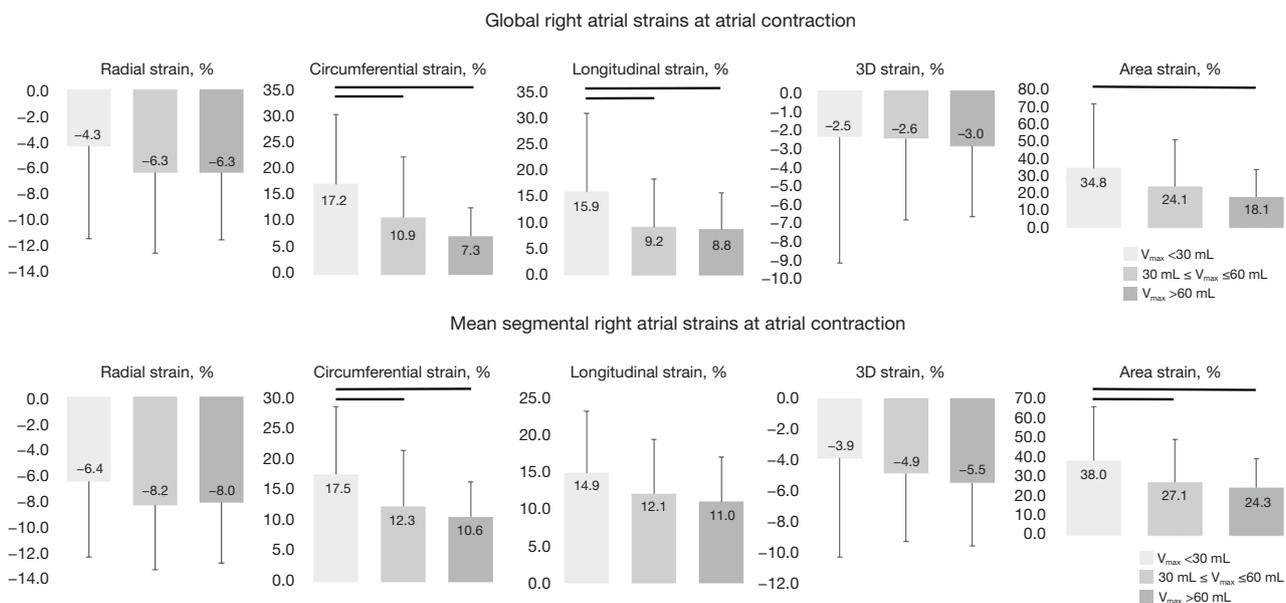
Global right atrial strains at atrial contraction

Mean segmental right atrial strains at atrial contraction

Figure 3 Global and mean segmental right atrial strains at atrial contraction are presented in different maximum right atrial volume groups. 3D, three-dimensional; V_{max}, maximum right atrial volume.

3DSTE seems to be capable of detailed assessment of volumetric and contractile RA features at the same time (13).

In a recent study, similar LA analysis was performed in healthy subjects by 3DSTE (3). Compared to these findings, RA functional properties showed different patterns with increasing RA volumes as compared to findings with LA (3). While atrial volumes and stroke volumes showed similar increase with increasing atrial volumes, emptying fractions in reservoir and booster pump functions remained unchanged for both atria. However, emptying fraction for
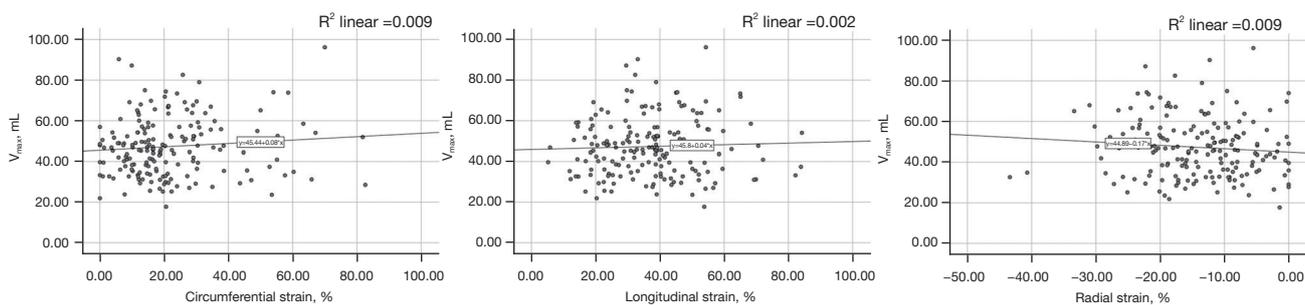
Figure 4 Linear regression between maximum right atrial volume and global peak radial, longitudinal and circumferential strains. V_{max}, maximum right atrial volume.
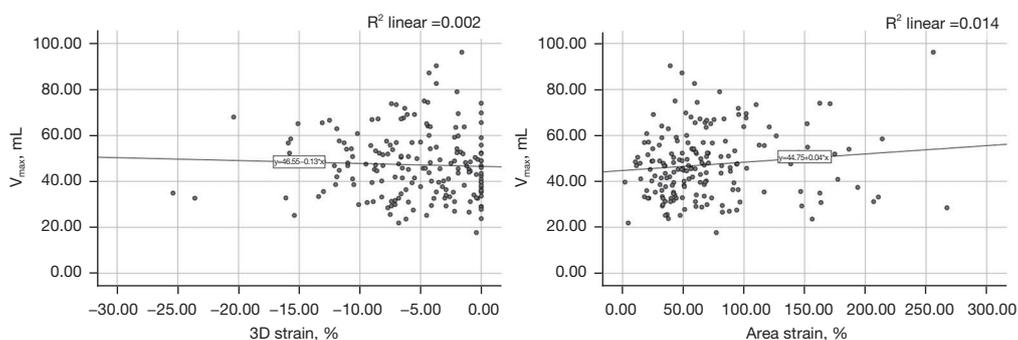

Figure 5 Linear regression between maximum right atrial volume and global peak area and three-dimensional strains. 3D, three-dimensional; V_{max}, maximum right atrial volume.

conduit function (PAEF) was significantly enhanced for RA and deteriorated for LA. When peak strains representing the systolic reservoir phase were assessed, LA-RS and LA-3DS were larger in healthy cases with larger LA volumes, but only up to a point, similar significant findings could not be detected with RA. RA-RS and RA-3DS showed non-significant increase with increasing RA volumes in healthy subjects. While CS and LS of both atria did not show relationship with increasing volumes, RA-AS was the highest when V_{max} was the highest. When atrial strains at atrial contraction were examined, LA-RS and LA-3DS behaved similarly to peak strains. Similar, but non-significant pattern could be detected for RA. While CS, LS and AS of LA did not change with increasing LA volumes, an obvious significant reduction with increasing volumes could be demonstrated for RA suggesting different behaviour of LA and RA with increasing atrial volumes.

The most important clinical implication of the study was that RA and LA seem to behave differently with increasing volumes with partially different atrial deformation response even in healthy circumstances. However, we could ask: what

could be the reason for these differences? RA and LA show alterations in their morphology, size and volume during the cardiac cycle with pressure and venous inflow (12,14). Atrioventricular valves (tricuspid *vs.* mitral valves) with their structural differences (for instance in the number of leaflets or in the length of papillary muscle and tendons) could affect the results as well (15,16). Essential differences in central pumps of the pulmonary (right ventricle-engined) and systemic (LV-engined) circuits are also known and well documented (11,17). However, further studies are warranted for better understanding the human physiology and pathophysiology of the RA for which novel non-invasive imaging methodologies like 3DSTE (or magnetic resonance imaging) theoretically make optimal opportunities.

Limitation section

There were several important limitations:

❖ Quality of 2D echocardiography-derived images is still better as compared to 3DSTE-derived ones due to lower temporal and spatial image resolutions for 3DSTE (5,6).

- ❖ 3DSTE has several technical issues including lower frame rate and most of transducers still have larger footprints as compared to those for 2D echocardiography, which could have effects on image quality and final results (5,6).
- ❖ Although 3DSTE-derived atrial volumes and strains are validated, more studies confirming its accuracy are warranted (13).
- ❖ RA appendage, caval veins and coronary sinus were excluded from the assessments, which could be realized when interpreting the results.
- ❖ Direct comparison of 2D echocardiography- and 3DSTE-derived RA parameters was not aimed to be performed.
- ❖ Moreover, volumetric and functional features of other cardiac chambers were also not examined (18,19).
- ❖ Only 3DSTE-derived RA volumes were measured. Featuring RA morphological abnormalities or measuring RA diameters or areas in selected planes were not aimed in this study.
- ❖ Although there can be a debate, that atrial septum is a part of which atrium, we considered it as a part of RA.
- ❖ Until now, exact 3DSTE-derived RA segmentation model is missing, therefore LV cast was used during the assessment (11).
- ❖ Although the pulmonary artery, pulmonary valve, right ventricle and RA form a functional unit, their combined effects were not examined in details which could be a basis of future investigations.

Conclusions

Increasing RA volumes do not cause significant increase in RA contractility represented by strains, but reduction in strains in longitudinal and circumferential directions could be detected in end-diastolic booster pump function. In contrast to LA, obvious signs of Frank-Starling mechanism could not be detected for RA.

Acknowledgments

Footnote

Conflicts of Interest: Both authors have completed the ICMJE uniform disclosure form (available at https://qims.amegroups. com/article/view/10.21037/qims-22-307/coif). AN serves as an unpaid editorial board member of *Quantitative Imaging in Medicine and Surgery*. The other author has no conflicts of interest to declare.

Ethical Statement: The authors are accountable for all aspects of the work in ensuring that questions related to the accuracy or integrity of any part of the work are appropriately investigated and resolved. The study was conducted in accordance with the Declaration of Helsinki (as revised in 2013). The study was approved by the Institutional and Regional Human Biomedical Research Committee of University of Szeged (Hungary) (No. 71/2011 and updated versions) and informed consent was taken from all the subjects.

References

1. Jacob R, Dierberger B, Kissling G. Functional significance of the Frank-Starling mechanism under physiological and pathophysiological conditions. Eur Heart J 1992;13 Suppl E:7-14.
2. Aurigemma GP, Zile MR, Gaasch WH. Contractile behavior of the left ventricle in diastolic heart failure: with emphasis on regional systolic function. Circulation 2006;113:296-304.
3. Nemes A, Kormányos Á, Domsik P, Kalapos A, Gyenes N, Lengyel C. Correlations between left atrial volumes and strains in healthy adults: Detailed analysis from the three-dimensional speckle-tracking echocardiographic MAGYAR-Healthy Study. J Clin Ultrasound 2021;49:650-8.
4. Anwar AM, Geleijnse ML, Soliman OI, Nemes A, ten Cate FJ. Left atrial Frank-Starling law assessed by real-time, three-dimensional echocardiographic left atrial volume changes. Heart 2007;93:1393-7.
5. Nemes A, Kalapos A, Domsik P, Forster T. Three-dimensional speckle-tracking echocardiography -- a further step in non-invasive three-dimensional cardiac

imaging. Orv Hetil 2012;153:1570-7.

6. Urbano-Moral JA, Patel AR, Maron MS, Arias-Godinez JA, Pandian NG. Three-dimensional speckle-tracking echocardiography: methodological aspects and clinical potential. Echocardiography 2012;29:997-1010.

7. Ammar KA, Paterick TE, Khandheria BK, Jan MF, Kramer C, Umland MM, Tercius AJ, Baratta L, Tajik AJ. Myocardial mechanics: understanding and applying three-dimensional speckle tracking echocardiography in clinical practice. Echocardiography 2012;29:861-72.

8. Nemes A, Kormányos Á, Domsik P, Kalapos A, Ambrus N, Lengyel C. Normal reference values of three-dimensional speckle-tracking echocardiography-derived right atrial volumes and volume-based functional properties in healthy adults (Insights from the MAGYAR-Healthy Study). J Clin Ultrasound 2020;48:263-8.

9. Nemes A, Kormányos Á, Domsik P, Kalapos A, Ambrus N, Lengyel C, Forster T. Normal reference values of right atrial strain parameters using three-dimensional speckle-tracking echocardiography (results from the MAGYAR-Healthy Study). Int J Cardiovasc Imaging 2019;35:2009-18.

10. Kormányos Á, Kalapos A, Domsik P, Gyenes N, Ambrus N, Valkusz Z, Lengyel C, Nemes A. The right atrium in acromegaly-a three-dimensional speckle-tracking echocardiographic analysis from the MAGYAR-Path Study. Quant Imaging Med Surg 2020;10:646-56.

11. Lang RM, Badano LP, Mor-Avi V, Afilalo J, Armstrong A, Ernande L, Flachskampf FA, Foster E, Goldstein SA, Kuznetsova T, Lancellotti P, Muraru D, Picard MH, Rietzschel ER, Rudski L, Spencer KT, Tsang W, Voigt JU. Recommendations for cardiac chamber quantification by echocardiography in adults: an update from the American Society of Echocardiography and the European Association of Cardiovascular Imaging. Eur Heart J Cardiovasc Imaging 2015;16:233-70.

12. Tadic M. The right atrium, a forgotten cardiac chamber: An updated review of multimodality imaging. J Clin Ultrasound 2015;43:335-45.

13. Nemes A, Forster T. Echocardiographic evaluation of the right atrium - from M-mode to 3D speckle-tracking imaging. Orv Hetil 2016;157:1698-707.

14. Hoit BD. Left atrial size and function: role in prognosis. J Am Coll Cardiol 2014;63:493-505.

15. Dal-Bianco JP, Levine RA. Anatomy of the mitral valve apparatus: role of 2D and 3D echocardiography. Cardiol Clin 2013;31:151-64.

16. Yucel E, Bertrand PB, Churchill JL, Namasivayam M. The tricuspid valve in review: anatomy, pathophysiology and echocardiographic assessment with focus on functional tricuspid regurgitation. J Thorac Dis 2020;12:2945-54.

17. Rudski LG, Lai WW, Afilalo J, Hua L, Handschumacher MD, Chandrasekaran K, Solomon SD, Louie EK, Schiller NB. Guidelines for the echocardiographic assessment of the right heart in adults: a report from the American Society of Echocardiography endorsed by the European Association of Echocardiography, a registered branch of the European Society of Cardiology, and the Canadian Society of Echocardiography. J Am Soc Echocardiogr 2010;23:685-713.

18. Nemes A, Kormányos Á, Domsik P, Ambrus N, Gyenes N, Vezendi K, Marton I, Borbényi Z. Left ventricular rotational abnormalities in hemophilia-insights from the three-dimensional speckle-tracking echocardiographic MAGYAR-Path Study. Quant Imaging Med Surg 2022;12:886-93.

19. Nemes A, Kormányos Á, Gyenes N, Ambrus N, Horváth Á, Lengyel C, Valkusz Z. Is treated hypopituitarism associated with increased left ventricular strains?-detailed analysis from the three-dimensional speckle-tracking echocardiographic MAGYAR-Path Study. Quant Imaging Med Surg 2022;12:838-45.